Sensitivity analysis of a simulation model for evaluating renewable distributed generation on a power network

Rodrigo Mena, Martin Hennebel, Enrico Zio

Sensitivity Analysis of a Simulation Model for Evaluating Renewable Distributed Generation on a Power Network

Rodrigo Mena[a], Martin Hennebel[b], Enrico Zio[ad]

[a]Chair on Systems Science and the Energetic Challenge, European Foundation for New Energy-Electricité de France, at École Centrale Paris - Supelec, Paris, France

[b]Supelec, Gif-sur-Yvette, France

[d]Politecnico di Milano, Milano, Italia

Abstract: We present a sensitivity analysis of a simulation model for the evaluation of the performance of a renewable distributed generation (DG) network. Uncertainties in renewable energy sources, components failure and repair events, loads and grid power supply are taken into account. The sensitivity analysis is performed individually with respect to the characteristic uncertain variables associated to each type of DG technology available. The impact of these uncertain variables is evaluated in terms of two performance functions, global cost (C_g) and energy not supplied (*ENS*). The results show the trends of performance of the DG-integrated network under different conditions. This allows evaluating the impact of the different DG technologies.

Keywords: distribution network, renewable energy generation, power flow, uncertainty, Monte Carlo simulation, sensitivity analysis

1. INTRODUCTION

DG is defined as 'an electric power source connected directly to the distribution network or on the customer site of the meter' [1-3]. Hypothetically, the fact that the power flows through shorter paths decreases the amount of unsatisfied power demands and reduces the power losses and voltages drops [4]. Additionally, the modular structure of the diverse types of DG technologies allows lower investment risks [5, 6].

The use of local renewable energy sources has become progressively more attractive for environmental sustainability (e.g. the Kyoto Protocol [3]). Technologies like wind turbines, photovoltaic panels and hydropower turbines, among others; make DG integration even more tempting.

Nonetheless, sizing and allocation of different types of DG units must be carefully planned in order not to incur in complications, such as reduction of power quality and reliability, degradation of protection and control devices, voltage instability, and the consequent negative economic impacts [7-10].

Modeling needs to be used to evaluate different alternatives of renewable DG integration, for the purpose of informing and supporting decision-making. A fundamental issue to consider is the treatment of the inherently uncertain behavior of the renewable energy sources, the stochastic occurrence of unexpected failures and stoppages of power grid components, the variability in the power demands and energy prices, the fluctuations in the available main power supply, the overloads and interruptions in the feeders, the failures in control and protection devices, etc.

In this paper, we adopt a combined Monte Carlo and optimal power flow (MCS-OPF) simulation framework for evaluating a renewable DG-integrated network, previously presented by the authors [11], and perform a sensitivity analysis over the uncertain variables, in order to evaluate their impact over the two performance functions considered, global cost (C_g) and energy not supplied (*ENS*).

2. RENEWABLE DG-INTEGRATED NETWORK SIMULATION MODEL

In this section, we present the MCS-OPF model. We do this with reference to a case study, and in the following we introduce the definition of the structure and configuration of the DG-integrated network, the uncertainty sources and their treatment, the random generation of operating scenarios and the formulation of the OPF. The outputs of the MCS-OPF model are the probability density functions of the network performance metrics, the C_g and *ENS*.

2.1 Renewable DG-Integrated Network Structure and Configuration

The exemplary DG-integrated network considers four types of components: renewable DG units, main power supply spots (MS), nodes and feeders. Renewable DG units and MS are power sources, and the nodes correspond to the locations at which the renewable DG units, MS and power loads are located. Feeders connect different nodes and through them the power is distributed. In Figure 1, a DG-integrated network is presented as example of configuration considered: it is an adaptation of the *IEEE 13 nodes test feeder*, for which the feeders with length equals to zero, the switch, regulator and capacitor are neglected.

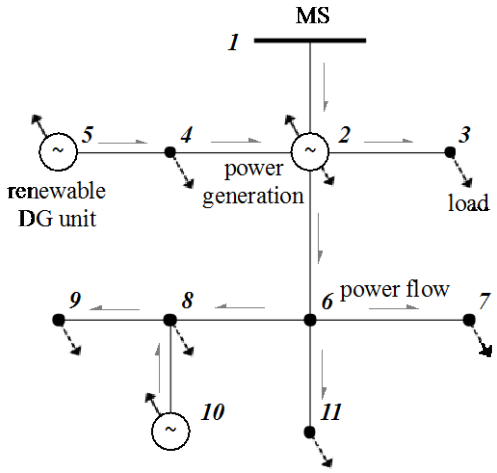

Figure 1. Example of a renewable DG-integrated network configuration

In this work, the renewable DG units are considered of four types of technologies: solar photovoltaic (PV), wind turbines (W), electric vehicles (EV) and storage devices (ST). Power generation interruptions due to failures are accounted for.

The notation used to indicate the sets and subsets of components of the DG-integrated network is:

- N set of all nodes.
  - $n = |N|$ number of nodes in the network.
- FD set of all feeders.
- MS set of all types of main power supply sources.
  - $m = |MS|$ number of main supply type (transformers).
- DG set of all DG technologies.
  - $d = |DG|$ number of DG technologies.
    - PV set of all photovoltaic technologies.
    - W set of all wind technologies.
    - EV set of all electric vehicle technologies.
    - ST set of all storage technologies.

To indicate the location and capacity size of the power sources (DG and MS), the configuration is represented in matrix form:

$$\Xi = \left[\begin{array}{ccccc|ccccc} \xi_{1,1} & \cdots & \xi_{1,j} & \cdots & \xi_{1,m} & \xi_{1,m+1} & \cdots & \xi_{1,m+j} & \cdots & \xi_{1,m+d} \\ \vdots & \ddots & \vdots & & \vdots & \vdots & \ddots & \vdots & & \vdots \\ \xi_{i,1} & \cdots & \xi_{i,j} & \cdots & \xi_{i,m} & \xi_{i,m+1} & \cdots & \xi_{i,m+j} & \cdots & \xi_{i,m+d} \\ \vdots & & \vdots & \ddots & \vdots & \vdots & & \vdots & \ddots & \vdots \\ \xi_{n,1} & \cdots & \xi_{n,j} & \cdots & \xi_{n,m} & \xi_{n,m+1} & \cdots & \xi_{n,m+j} & \cdots & \xi_{n,m+d} \end{array}\right] = \left[\Xi^{MS} \,\middle|\, \Xi^{DG}\right] \quad (1)$$

where,

Ξ configuration matrix of the type, size and location of the power sources present in the distribution network

- Ξ^{MS} allocated main supply part of the configuration matrix

Ξ^{DG} allocated DG part of the configuration matrix

$$\xi_{i,j} = \begin{cases} \zeta & \text{units of the MS type or DG technology allocated at node } i \\ 0 & \text{otherwise} \end{cases} \quad \forall i \in N, j \in MS \cup DG, \zeta \in Z^{+} \tag{2}$$

Feeders deployment is defined by the set of connected nodes:

$$FD = \{(1,2),\ldots,(i,i')\} \quad \forall (i,i') \in N \times N, (i,i') \text{ is a feeder} \tag{3}$$

Both power sources Ξ and feeders FD are subject to operational uncertainties, so that any time instant the actual performance of the network is strongly dependent on the current operational configuration and existing operating scenarios. Moreover, if the distribution network is a 'price taker', the economic conditions depend on the uncertain behavior of the power demand, directly impacting over the variability of the energy price [5, 12, 13].

2.2 Uncertainty Modeling

In the present framework, the network operation is characterized by the location and magnitude of the power available and the loads. Operational uncertainty is present because of uncertainty in the states of operation of the components, due to degradation and failures, and in the behavior of the renewable energy sources. These uncertainties have a direct impact on the power available (in the DG units, MS spots and/or FD) to satisfy power demands, which are, in turn, also subject to variability.

To emulate the operation of the DG-integrated network under these uncertain conditions, we adopt different stochastic models, as here reported by Table 1. For more information on the individual models, the interested reader can consult [11].

Table 1. Models adopted for describing the uncertain conditions of operation of the DG-integrated network

	Uncertain variable	Nomenclature	States and Units	Model	Parameters
Mechanical states of the components	Mechanical state	$mc_{i,j}$ $mc_{i,i'}$	(*0*): *under repair* (*1*): *operating*	Two-state Markov	λ_j^F, λ_j^R $\lambda_{i,i'}^F, \lambda_{i,i'}^R$
Main power supply	Available main power supply	P_i^{ms}	[*kW*]	Normal distribution truncated at zero and at the maximum capacity of the transformer	$\mu_i^{ms}, \sigma_i^{ms}$ P_{cap}^{ms}
Photovoltaic generation	Solar irradiance	s_i	[*0,1*]	Beta distribution	α_i, β_i
Wind generation	Wind speed	ws_i	[*m/s*]	Rayleigh distribution	σ_i
Electric vehicles	Operating state	$op_{t,j}$	(*-1*): *charging* (*0*): *disconnected* (*1*): *discharging*	'Block groups' Hourly probability distribution of EV operating states per day	t_d
Storage devices	Level of charge	$Q_{i,j}^{st}$	[*kJ*]	Uniform distribution	$M_{T_{i,j}}, SE_j$
Power demand	Nodal power demand	L_i	[*kW*]	Daily nodal load profiles, hourly normally distributed load. Normal distribution truncated at zero	μ_i, σ_i

where $\forall i,i' \in N, j \in MS \cup DG, (i,i') \in FD$,

λ_j^F, λ_j^R failure and repair rates of power source *j*, respectively.

$\lambda_{i,i'}^F, \lambda_{i,i'}^R$ failure and repair rates of feeder (*i,i'*), respectively.

$\mu_i^{ms}, \sigma_i^{ms}$ Normal distribution mean and standard deviation associated to the main supply at node *i*.

P_{cap}^{ms} maximum capacity of the transformer [*kW*].

α_i, β_i parameters of the Beta probability density function at node *i*.

σ_i scale parameter of the Rayleigh distribution function at node *i*.

t_d hour of the day [*h*], randomly sampled from a uniform distribution *U*(*1,24*).

$M_{T_{i,j}}, SE_j$ mass of active chemical in the battery type *j* at node *i* and specific energy of the active chemical in

the battery type *j* [*kJ/kg*].

The power available in the power sources (MS and DG) depends on the corresponding state of operation and power output function. In the case of MS spots, the power output is directly the uncertain variable P^{ms}, whereas for each DG technology the power output is a function of the corresponding uncertain variable that represents the behavior of the energy source: solar irradiance, wind speed, EV operating states and level of charge in the batteries. In addition, the power output functions depend on specific technical parameters given by each type of DG technology devices, such as, solar cells, wind turbines, EV types and batteries active chemical. The power output functions for the DG technologies under consideration are summarized in Table 2. More information can be found in [11].

Table 2. Power output functions of the DG technologies considered

DG Technology	Power output function	Nomenclature
PV	$P^{pv}(s) = n_{cells} \times FF \times V \times I$ (4)	T_a ambient temperature [^oC] N_{oT} nominal cell operating temperature [^oC] T_c cell temperature [^oC] I_{sc} short circuit current [*A*] k_i current temperature coefficient [*mA/°C*] V_{oc} open circuit voltage [*V*] k_v voltage temperature coefficient [*mV/°C*] V_{MPP} voltage at maximum power [*V*] I_{MPP} current at maximum power [*A*] *FF* fill factor n_{cells} number of photovoltaic cells $P^{pv}(s)$ PV power output [*W*]
	$T_c = T_a + s\left(\frac{N_{oT} - 20}{0.8}\right)$	
	$I = s\left(I_{sc} + k_i\left(T_c - 25\right)\right)$	
	$V = V_{oc} + k_v T_c$	
	$FF = \frac{V_{MPP} I_{MPP}}{V_{oc} I_{sc}}$	
W	$P^w(ws) = \begin{cases} P^w_{RTD}\frac{(ws - ws_{ci})}{(ws_a - ws_{ci})} & ws_{ci} \le ws < ws_a \\ P^w_{RTD} & ws_a \le ws < ws_{co} \\ 0 & otherwise \end{cases}$ (5)	ws_{ci} cut-in wind speed [*m/s*] ws_a rated wind speed [*m/s*] ws_{co} cut-out wind speed [*m/s*] P^w_{RTD} rated power [*kW*] $P^w(ws)$ wind power output [*kW*]
EV	$P^{ev}(op) = \begin{cases} P^{ev}_{RTD} & op = 1 \\ 0 & op = 0 \\ -P^{ev}_{RTD} & op = -1 \end{cases}$ (6)	t_{Rop} residence interval for operating state *op* [*h*] P^{ev}_{RTD} rated power [*kW*]
ST	$P^{st}(t_R) = P^{st}_{RTD} \quad \forall t_R \in [0, t'_R]$ (7)	P^{st}_{RTD} rated power [*kW*] t'_R discharging time interval [*h*]
	$t'_R(Q^{st}) = \frac{Q^{st}}{P^{st}_{RTD}}$	

2.3 Monte Carlo – Optimal Power Flow Simulation

MCS has already been used for evaluating the performance of power distribution networks [10, 14-18]. In particular, sequential, pseudo-sequential and non-sequential MCS have been implemented to emulate the stochastic operational scenarios of power generation and load demands in distribution networks. In the present paper, non-sequential MCS is used to randomly sample the uncertain variables, without dependence of previous operating conditions.

2.3.1 Sampling process

For the given DG-integrated network with structure and configuration {*Ξ,FD*}, each uncertain variable is randomly sampled. We indicate by vector $\vec{g}$ the resulting realization of the operational scenario. Thus, {*Ξ,FD*} and $\vec{g}$

characterize the conditions of the network operation in terms of location and magnitudes of the power available in the power sources (MS and DG) and loads. Then, the performance of the distribution network is evaluated through the OPF model. Figure 2 shows the diagram of the sampling process.

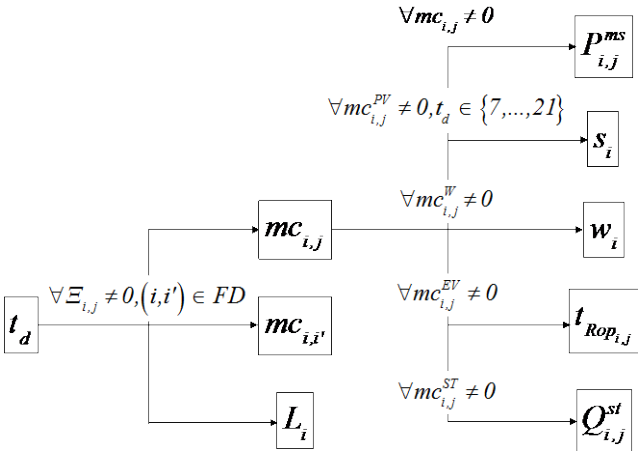

Figure 2. Sampling process diagram

$$\vec{\vartheta} = \left[t_d, P^{ms}_{i,j}, L_i, s_i, ws_i, t_{Rop_{i,j}}, Q^{st}_{i,j}, mc_{i,j}, mc_{i,i'} \right] \quad \forall i,i' \in N, j \in MS \cup DG, (i,i') \in FD \tag{8}$$

2.3.2 Optimal power flow formulation

Power flow analysis is performed by DC modeling, which accounts solely for active power flows, neglects power losses and assumes the voltage of the network as constant [19]. For a given configuration {*Ξ,FD*} and operational scenario $\vec{\vartheta}$ the formulation of the OPF problem is:

$$min \quad C^{net\vec{\vartheta}}_{O\&M}\left(P^{\vec{\vartheta}}_{Gu}\right) = \sum_{i \in N} \sum_{j \in MS \cup DG} C_{O\&M^v_j} \times P^{\vec{\vartheta}}_{Gu_{i,j}} \times t^S \tag{9}$$

s.t.

$$\left(\sum_{j \in MS \cup DG} P^{\vec{\vartheta}}_{Gu_{ij}} + LS^{\vec{\vartheta}}_i + \sum_{i' \in N} mc^{\vec{\vartheta}}_{i,i'} B_{i,i'} \left(\delta^{\vec{\vartheta}}_i - \delta^{\vec{\vartheta}}_{i'} \right) \right) - L^{\vec{\vartheta}}_i = 0 \quad \forall i,i' \in N, (i,i') \in FD \tag{10}$$

$$P^{\vec{\vartheta}}_{Gu_{i,j}} \leq P^{\vec{\vartheta}}_{Ga_{i,j}} \quad \forall i \in N, j \in MS \cup DG \tag{11}$$

$$0 \leq P^{\vec{\vartheta}}_{Gu_{i,j}} \quad \forall i \in N, j \in MS \cup DG \tag{12}$$

$$mc^{\vec{\vartheta}}_{i,i'} B_{i,i'} \left(\delta^{\vec{\vartheta}}_i - \delta^{\vec{\vartheta}}_{i'} \right) \leq V \times Amp_{i,i'} \quad \forall i,i' \in N, (i,i') \in FD \tag{13}$$

$$-mc^{\vec{\vartheta}}_{i,i'} B_{i,i'} \left(\delta^{\vec{\vartheta}}_i - \delta^{\vec{\vartheta}}_{i'} \right) \leq V \times Amp_{i,i'} \quad \forall i,i' \in N, (i,i') \in FD \tag{14}$$

where,

t^S	duration of the scenario [*h*].
$C^{net\vec{\vartheta}}_{O\&M}$	operating and maintenance costs of the total power supply and generation [*$*].
$C_{O\&M^v_j}$	operating and maintenance variable costs of the power source *j* [*$/kWh*].
$mc^{\vec{\vartheta}}_{i,i'}$	mechanical (operational) state of the feeder (*i,i'*).
$B_{i,i'}$	susceptance of the feeder (*i,i'*), [*1/Ω*].

$mc_{i,j}^{\vec{\vartheta}}$	mechanical (operational) state of the power source *j* at node *i*.
$P_{Ga_{i,j}}^{\vec{\vartheta}}$	available power in the source *j* at node *i* [*kW*].
$P_{Gu_{i,j}}^{\vec{\vartheta}}$	power produced by source *j* at node *i* [*kW*].
$LS_i^{\vec{\vartheta}}$	load shedding at node *i* [*kW*].
V	nominal voltage of the network [*kV*].
$Amp_{i,i'}$	ampacity of the feeder (*i*,*i'*), [*A*].

The load shedding in the node *i*, LS_i, is defined as the amount of load disconnected in node *i* to alleviate overloaded feeders and/or balance the demand of power with the available power supply [20].

The OPF objective is the minimization of the operating and maintenance costs associated to the generation of power for a given scenario $\vec{\vartheta}$ of duration t^S. Equation (10) corresponds to the power balance equation at node *i*, whereas equations (11) and (12) are the bounds of the power generation and equations (13) and (14) are the constraints that take into account the technical limits of the feeders.

The available power in the distribution network is a function of the configuration Ξ and operational states of the power sources:

$$P_{Ga_{i,j}}^{\vec{\vartheta}} = \xi_{i,j} mc_{i,j}^{\vec{\vartheta}} G_{i,j}^{\vec{\vartheta}} \tag{15}$$

where, $G_{i,j}^{\vec{\vartheta}}$ represents the unitary power output and depends on the type of power source, i.e.,

$$G_{i,j}^{\vec{\vartheta}} = \begin{cases} P_{i,j}^{ms}\left(mc_{i,j}^{\vec{\vartheta}}\right) & j \in MS \\ P_{i,j}^{pv}\left(s_i^{\vec{\vartheta}}, mc_{i,j}^{\vec{\vartheta}}\right) & j \in PV \\ P_{i,j}^{w}\left(ws_i^{\vec{\vartheta}}, mc_{i,j}^{\vec{\vartheta}}\right) & j \in W \quad \forall i \in N \\ P_{i,j}^{ev}\left(op\left(t_d^{\vec{\vartheta}}\right), t^{\vec{\vartheta}}{}_{Rop}, mc_{i,j}^{\vec{\vartheta}}\right) & j \in EV \\ P_{i,j}^{st}\left(Q^{st\vec{\vartheta}}, mc_{i,j}^{\vec{\vartheta}}\right) & j \in ST \end{cases} \tag{16}$$

2.4 Performance Evaluation of the DG-Integrated Network

Given a set Υ of *ns* sampled operational scenarios $\vec{\vartheta}_\ell$, $\ell \in \{1,\ldots, ns\}$, the OPF is solved for each scenario $\vec{\vartheta}_\ell \in \Upsilon$, giving in output the values of *ENS* and global cost.

2.4.1 Energy not supplied

ENS is a common index for reliability evaluation in power systems [20]. In the present work, its value is obtained directly from the OPF output in the form of the aggregation of all-nodal load sheddings per scenario $\vec{\vartheta}_\ell$:

$$ENS^{\vec{\vartheta}_\ell} = \sum_{i \in N} LS_i^{\vec{\vartheta}_\ell} \times t^s \quad \forall \vec{\vartheta}_\ell \in \Upsilon \tag{17}$$

$$ENS^{\Upsilon} = \left[ENS^{\vec{\vartheta}_1}, \ldots ENS^{\vec{\vartheta}_\ell}, \ldots ENS^{\vec{\vartheta}_{ns}}\right] \tag{18}$$

2.4.2 Global cost

The C_g of the distribution network is formed by two terms. The first one is composed by the investment-installation and the operation-maintenance fixed costs that are prorated hourly over the life of the project (horizon of analysis). The second includes the variable term related to the operating and maintenance costs. Note that the variable costs depend on power generation and supply, and correspond to the outputs of the OPF (equation (9)). In addition, this term considers revenues associated to the renewable sources incentives. Considering the distribution network as a 'price taker' entity, the profits depend on the value of the energy price that is correlated with the total load in the network. Three different ranges of load are considered for the daily profile. For each range, a correlation value of energy price is considered as shown in Figure 3(A).

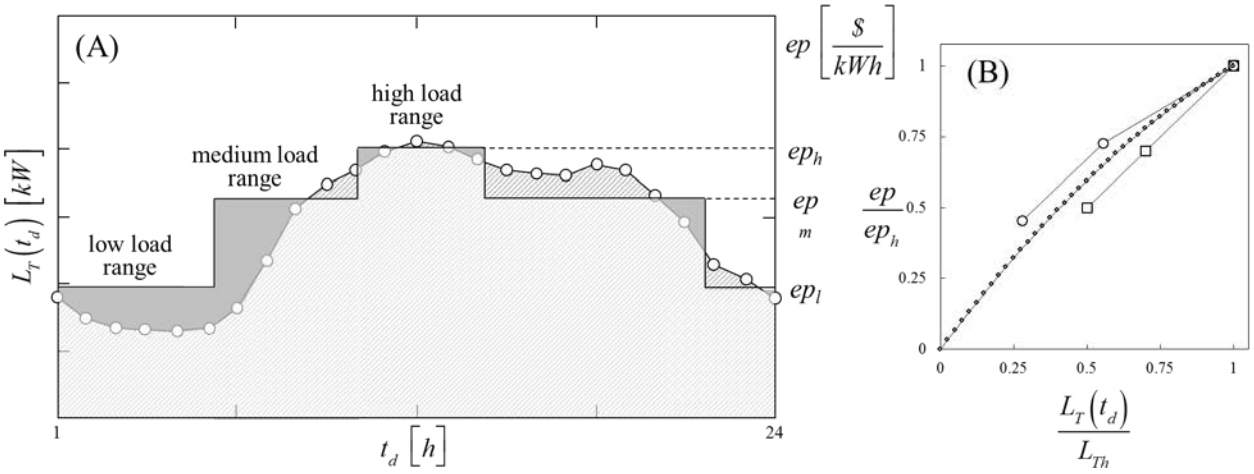

Figure 3. Example of load ranges definition for a generic daily load profile (A) and correlation energy price-total load (B) [5, 12, 13]

In Figure 3(B) the correlation between energy price and total load is presented as the proportion of their maximum values. As an intermediate approximation of existing studies (e.g. [5, 12, 13]), the line with square-markers represents the proportional correlation used in this study, which can be expressed as:

$$ep = ep_h \left[-0.38 \left(\frac{L_T(t_d)}{L_{Th}} \right)^2 + 1.38 \frac{L_T(t_d)}{L_{Th}} \right] \tag{19}$$

Thereby, the global cost function for a scenario $\vec{\vartheta}_t$ is given by:

$$C_g^{\vec{\vartheta}_t} = \frac{\sum_{i \in N} \sum_{j \in DG} \xi_{i,j} \left(C_{inv_j} + C_{O\&M_j^f} \right)}{t^h} \times t^S + C_{O\&M}^{net,\vec{\vartheta}_t} - \left(inc + ep\left(L_T^{\vec{\vartheta}_t} \right) \right) \times \sum_{i \in N} \sum_{j \in DG} P_{Gu_{i,j}}^{\vec{\vartheta}_t} \times t^S \quad \forall \vec{\vartheta}_t \in \Upsilon \tag{20}$$

$$\overrightarrow{C_g}^{\Upsilon} = \left[C_g^{\vec{\vartheta}_1}, ..., C_g^{\vec{\vartheta}_t}, ..., C_g^{\vec{\vartheta}_{n^t}} \right] \tag{21}$$

where,

C_{inv_j}	investment cost of the DG technology *j* [$].
$C_{O\&M_j^f}$	operating and maintenance fixed costs of the DG technology *j* [$].
t^h	horizon of analysis [*h*].
inc	incentive for generation from renewable sources [*$/kWh*].
ep	energy price [*$/kWh*].
$C_g^{\vec{\vartheta}_t}$	global cost [$].

Figure 4 shows the flowchart of the complete MCS-OPF framework.

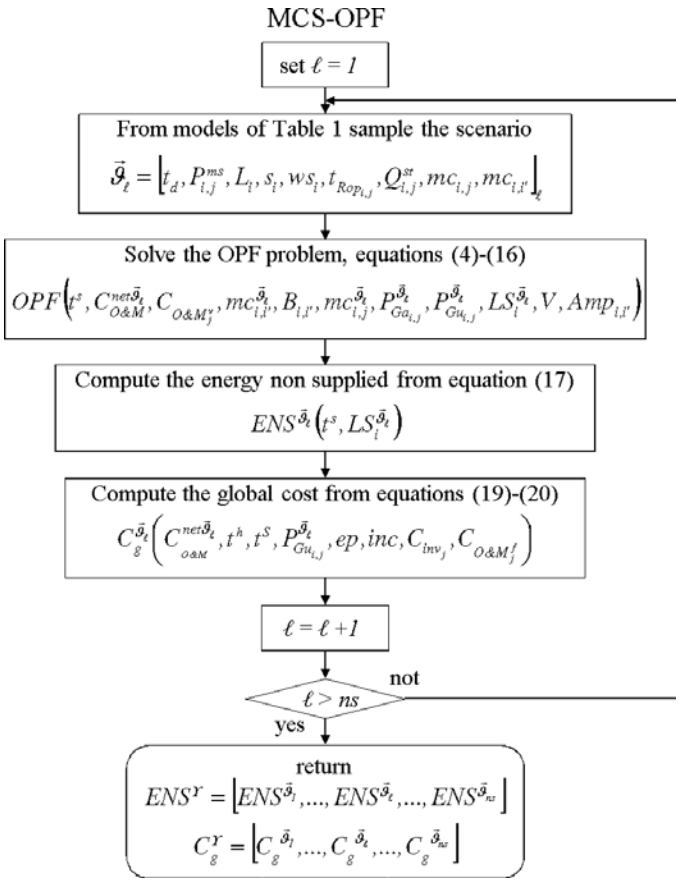

Figure 4. MCS-OPF flow chart

Finally, the sampled distributions of the performance outcomes vectors ENS^Υ and C^Υ_g of the MCS-OPF applied to the set of scenarios Υ are considered as approximations of the probability density functions of *ENS* and C_g, respectively.

3. APPLICATION

We consider a distribution network adapted from the *IEEE 13 nodes test feeder* [21, 22]. The original spatial structure is maintained the same but the feeders of length zero, the regulator, capacitor and switch are neglected. Even though the network is small, it presents the relevant characteristics of interest for the analysis, e.g. the presence of a main power supply spot and comparatively low and high spot and distributed load values [22]. The original design of the *IEEE 13 nodes test feeder* is such that the total power demands are satisfied without overloaded feeders: we modify it so that it becomes of interest to consider the integration of renewable DG units. Specifically, the location and values of some of the load spots and the ampacity values of some feeders have been modified in order to generate conditions of power congestion of the lines, leading to shortages of power supply to specific portions of the network.

3.1 DG-Integrated Network Description

The distribution network presents a radial structure of $n = 11$ nodes and $fd = (n-1) = 10$ feeders, as shown in Figure 5. The nominal voltage is $V = 4.16$ [kV], constant for the resolution of the DC optimal power flow problem (Subsection 2.3).

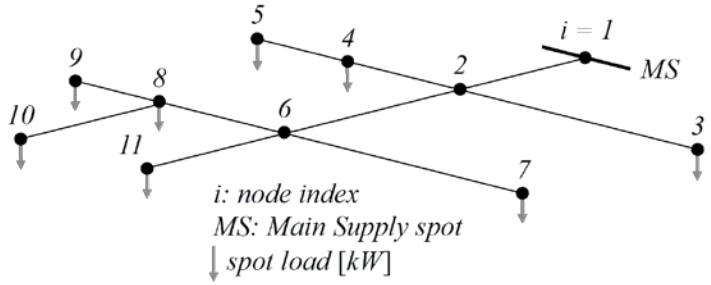

Figure 5. Radial 11-nodes distribution network

Table 3 contains the technical characteristics of the different types of feeders considered: specifically, the indexes of the pairs of nodes that are connected by each feeder of the network, their length, reactance *X* and their ampacity *Amp*.

Table 3. Feeders characteristic and technical data [21]

type	*node i*	*node i'*	*length* [*km*]	*X* [*Ω/km*]	*Amp* [*A*]
T1	*1*	*2*	*0.610*	*0.371*	*365*
T2	*2*	*3*	*0.152*	*0.472*	*170*
T3	*2*	*4*	*0.152*	*0.555*	*115*
T1	*2*	*6*	*0.610*	*0.371*	*365*
T3	*4*	*5*	*0.091*	*0.555*	*115*
T6	*6*	*7*	*0.152*	*0.252*	*165*
T4	*6*	*8*	*0.091*	*0.555*	*115*
T1	*6*	*11*	*0.305*	*0.371*	*365*
T5	*8*	*9*	*0.091*	*0.555*	*115*
T7	*8*	*10*	*0.244*	*0.318*	*115*

Concerning the main power supply spot, the maximum active power capacity of the transformer and the parameters of the normal distribution that describe its variability are given in Table 4.

Table 4. Main power supply parameters

node	P_{cap}^{ms} [*kW*]	*Normal*	
		μ^{ms}	σ^{ms}
1	*1600*	*1200*	*27.5*

The nodal power demands are reported as daily profiles, normally distributed on each hour. The mean μ and variance σ values of the nodal daily profiles of the power demands are shown in Figure 6(A) and (B), respectively.

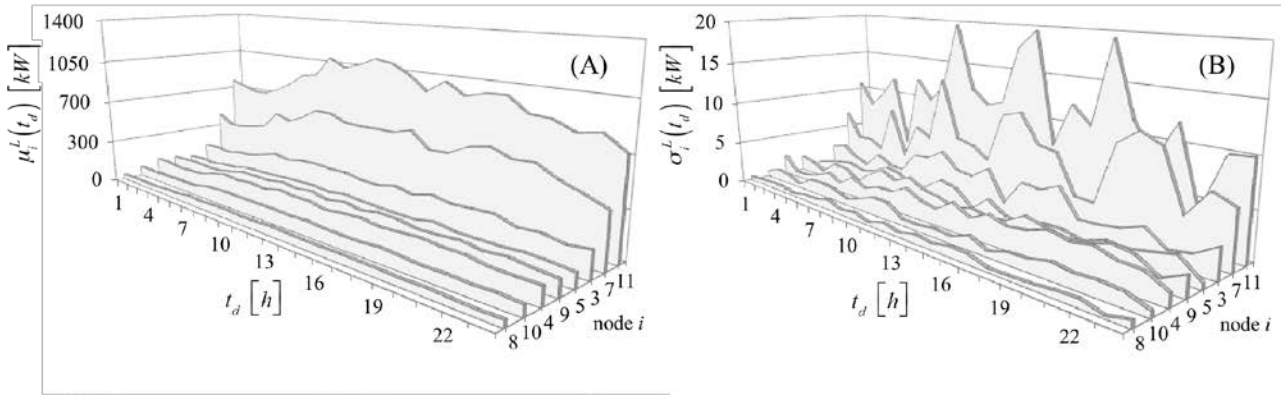

Figure 6. Mean (A) and variance (B) values of nodal power demand daily profiles

The technical parameters of the four different types of DG technologies available to be integrated into the distribution network (PV, W, EV and ST) are given in Table 5. The values of the parameters of the Beta and Rayleigh distributions describing the variability of the solar irradiation and wind speed (Table 1), are assumed constant in the whole network, i.e., the region of distribution is such that the weather conditions are the same for all nodes. The hourly per day operating states probability profile of the EV is presented in Figure 7.

Table 5. Parameters of PV, W, EV and ST technologies [4, 5, 17]

PV	
Beta distr. α	*0.26*

W	
Rayleigh dist. σ	*7.96*

EV	
P_{RTD}^{ev} [*kW*]	*6.30*

Beta distr. β	*0.73*
W_{peak} [*kW*]	*0.05*
T_a [*ºC*]	*30.00*
N_{oT} [*ºC*]	*43.00*
I_{sc} [*A*]	*1.80*
k_i [*mA/ºC*]	*1.40*
V_{oc} [*V*]	*55.50*
k_v [*mV/ºC*]	*194.00*
V_{MPP} [*V*]	*38.00*
I_{MPP} [*A*]	*1.32*

P^{w}_{RTD} [*kW*]	*50.00*
ws_{ci}	*3.80*
ws_{a}	*9.50*
ws_{co}	*23.80*

ST	
P^{st}_{RTD} [*kW/kg*]	*0.275*
SE [*kJ/kg*]	*0.042*

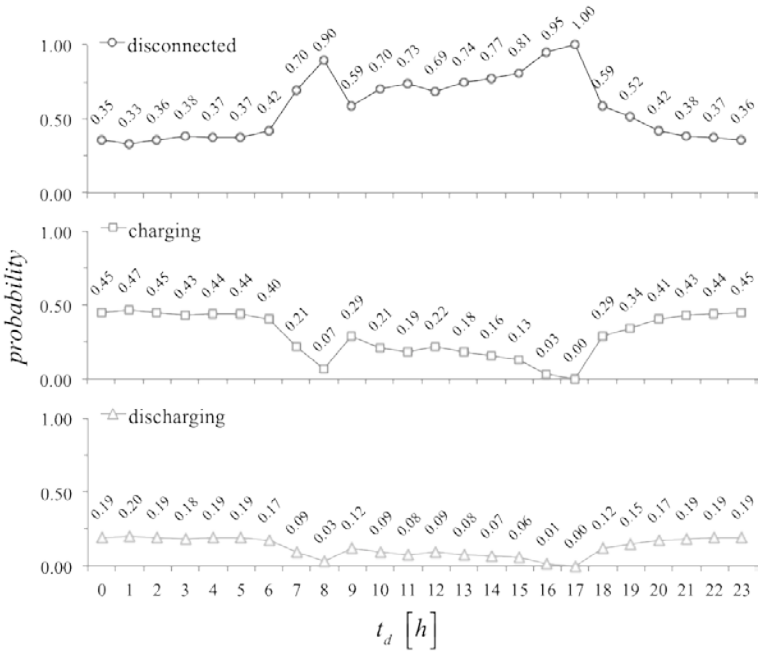

Figure 7. Hourly per day probability data of EV operating states

Failure and repair rates of the components of the distribution network are provided in Table 6 and Table 7, respectively.

Table 6. Failure rates of feeders, MS and DG units [4, 5, 17, 23]

type		λ^F [*failures/h*]	
		MS∪DG	*FD*
MS	*T1*	*0.000333*	*0.000333*
PV	*T2*	*0.000405*	*0.000405*
W	*T3*	*0.000355*	*0.000355*
EV	*T4*	*0.000355*	*0.000355*
ST	*T5*	*0.000355*	*0.000355*
-	*T6*	-	*0.000400*
-	*T7*	-	*0.000355*

Table 7. Repair rates of feeders, MS and DG units [4, 5, 17, 23]

type		λ^R [repairs/h]	
		MS∪DG	FD
MS	T1	0.0206	0.1980
PV	T2	0.0130	0.1620
W	T3	0.0149	0.1850
EV	T4	0.1050	0.1850
ST	T5	0.0730	0.1850
-	T6	-	0.1640
-	T7	-	0.1850

The values of the investment (C_{inv}), and fixed and variable Operational and Maintenance costs ($C_{O\&M^f}$ and $C_{O\&M^v}$) of the MS and DG units are reported in Table 8. The value of the incentive for renewable *kWh* supplied is taken as *0.024* [*$/kWh*] [24]. The maximum value of the energy price ep_h is *0.11*[*$/kWh*] [12, 13].

Table 8. Investment, fixed O&M and variable O&M costs of MS and DG [23-25]

type	$C_{inv}+C_{O\&M^f}$ [$]	$C_{O\&M^v}$ [$/kWh]
MS	-	0.1450000
PV	48.00	0.0000376
W	113750.00	0.0390000
EV	17000.00	0.0220000
ST	135.15	0.0000462

Three configurations Ξ^{DG} have been considered among those of the Pareto set obtained in [11] by the multi-objective optimization (MOO) by non-dominated sorting genetic algorithm (NSGA-II), with objectives the minimization of the expected energy not supplied *EENS* and expected global cost EC_g [11] (Figure 8). The configurations are those with minimum values of the objective functions and the third configuration is an intermediate solution of compromise of the two objectives. Tables 9, 10 and 11 summarize the three distributed configurations of power sources (including MS) and their expected available power output.

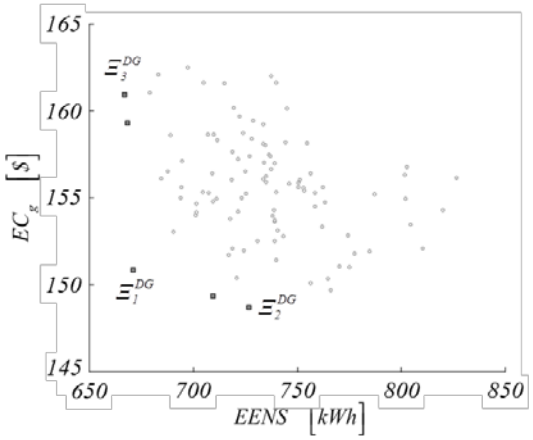

Figure 8. Pareto Front resulting from the MOO concerning the simultaneous minimization of *EENS* and EC_g [11]

Table 9. Configuration of power sources and expected power output of DG-integrated network Ξ_1^{DG} [11]

	Ξ^{MS}	Ξ_1^{DG}				EP_a^{ms}	$EP_{a_1}^{dg}$			
node	MS	PV	W	EV	ST	MS	PV	W	EV	ST
1	1	3100	0	0	700	1200.00	35.65	0.00	0.00	14.00
2	0	200	0	0	2050	0.00	2.30	0.00	0.00	41.00
3	0	50	0	0	800	0.00	0.58	0.00	0.00	16.00
4	0	2100	2	1	150	0.00	24.15	73.00	0.85	3.00

5	0	400	0	0	2000	0.00	4.60	0.00	0.00	40.00
6	0	1050	1	3	700	0.00	12.08	36.50	2.56	14.00
7	0	50	0	0	400	0.00	0.58	0.00	0.00	8.00
8	0	4750	2	0	100	0.00	54.63	73.00	0.00	2.00
9	0	50	0	0	100	0.00	0.58	0.00	0.00	2.00
10	0	0	0	0	750	0.00	0.00	0.00	0.00	15.00
11	0	1250	0	0	50	0.00	14.38	0.00	0.00	1.00

Table 10. Minimum EC_g configuration of power sources and expected power output of DG-integrated network Ξ_2^{DG} [11]

	Ξ^{MS}	Ξ_2^{DG}				EP_a^{ms}	$EP_{a_2}^{dg}$			
node	MS	PV	W	EV	ST	MS	PV	W	EV	ST
1	1	3100	0	0	0	1200.00	35.65	0.00	0.00	0.00
2	0	2350	0	0	2050	0.00	27.03	0.00	0.00	41.00
3	0	750	0	0	0	0.00	8.63	0.00	0.00	0.00
4	0	750	2	0	1450	0.00	8.63	73.00	0.00	29.00
5	0	700	0	0	900	0.00	8.05	0.00	0.00	18.00
6	0	1400	1	0	1400	0.00	16.10	36.50	0.00	28.00
7	0	0	0	2	400	0.00	0.00	0.00	1.71	8.00
8	0	1150	2	0	950	0.00	13.23	73.00	0.00	19.00
9	0	0	0	0	850	0.00	0.00	0.00	0.00	17.00
10	0	0	0	0	0	0.00	0.00	0.00	0.00	0.00
11	0	0	0	0	0	0.00	0.00	0.00	0.00	0.00

Table 11. Minimum *EENS* configuration of power sources and expected power output of DG-integrated network Ξ_3^{DG} [11]

	Ξ^{MS}	Ξ_3^{DG}				EP_a^{ms}	$EP_{a_3}^{dg}$			
node	MS	PV	W	EV	ST	MS	PV	W	EV	ST
1	1	1050	0	6	50	1200.00	12.08	0.00	5.12	1.00
2	0	200	0	0	0	0.00	2.30	0.00	0.00	0.00
3	0	50	0	7	1550	0.00	0.58	0.00	5.97	31.00
4	0	2100	2	0	1600	0.00	24.15	73.00	0.00	32.00
5	0	400	0	0	2000	0.00	4.60	0.00	0.00	40.00
6	0	1050	0	3	300	0.00	12.08	0.00	2.56	6.00
7	0	50	0	0	450	0.00	0.58	0.00	0.00	9.00
8	0	4750	2	0	750	0.00	54.63	73.00	0.00	15.00
9	0	750	1	0	0	0.00	8.63	36.50	0.00	0.00
10	0	0	0	0	500	0.00	0.00	0.00	0.00	10.00
11	0	1250	0	0	0	0.00	14.38	0.00	0.00	0.00

3.2 Sensitivity Analysis

A sensitivity analysis is performed considering PV, W and ST technologies. Then, the solar irradiance *s*, the wind speed *ws* and the storage level of one block of storage devices Q^{st} are the uncertain variables of interest. The impact of EV on the performance of the DG-integrated network is not analyzed, considering the higher probabilities that EV is in disconnected or charging states, and that when EV is disconnected its benefits are null and when charging it acts as a load, implying effects in opposition to those desired [11]. The blocks of storage devices considered are defined by the coordinates $\Xi_{1_{2,4}}^{DG}$, $\Xi_{2_{8,4}}^{DG}$ and $\Xi_{3_{1,4}}^{DG}$, which correspond to *2050*, *950* and *50* [kg] of batteries, respectively (Tables 9, 10, 11).

A total of *ns = 25000* operating scenarios have been simulated, whose results have been grouped according to the values of each of the three variables *s, ws* and Q^{st}, independently. For this, the interval [0,1] is divided into *40* bins of length *0.025*, defining *40* groups and assigning the results of the scenarios characterized by proportional values of the variables sampled $\{s/s_{max}, ws/ws_{max}, Q^{st}/Q^{st}_{max}\}$ to their corresponding group. The sequence of bins corresponds to increments of the *2.5%* of the variables $\{s, ws, Q^{st}\}$ relative to their maximum values.

3.3 Results and Discussion

The aggregated behavior of the sampled nodal power demands L_i [*kW*] (total load), from the simulation of each of the three DG-integrated network configurations, is shown in Figure 9. The breakdown in overall total load during day and night is also presented.

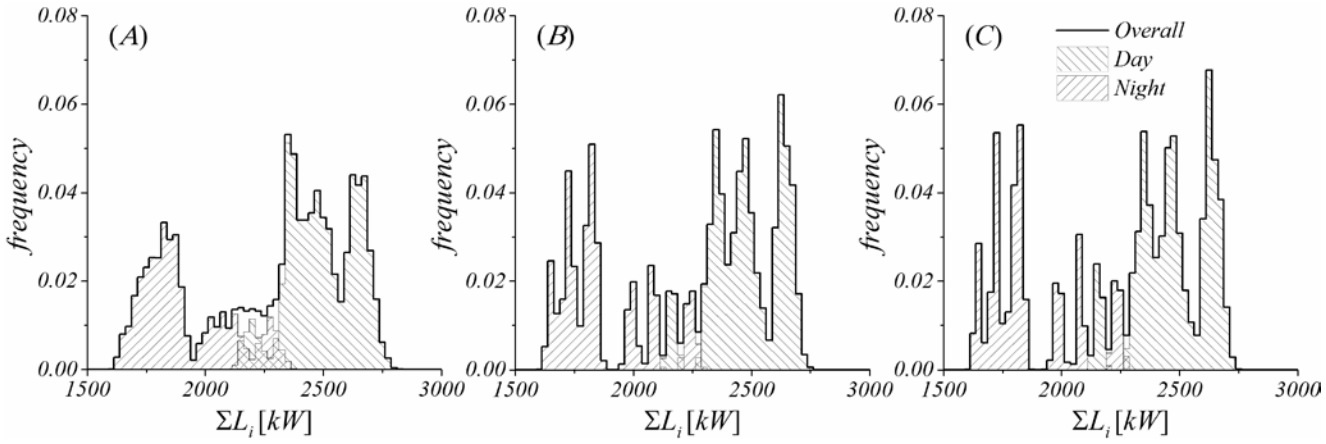

Figure 9. Total load behavior for each DG-integrated network configuration: Ξ_3^{DG} (*A*), Ξ_1^{DG} (*B*) and Ξ_2^{DG} (*C*)

The total load is composed of three main peaks. The first peak (*1500-2000* [*kW*]) corresponds to the low power demand range during the night, between *24.00* and *06.00* hours. The second and third peaks represent the high ranges of load (*2250-2500* and *2500-2750* [*kW*], respectively), which take place within the intervals *11.00-15.00* and *18.00-22.00* hours during the day, respectively.

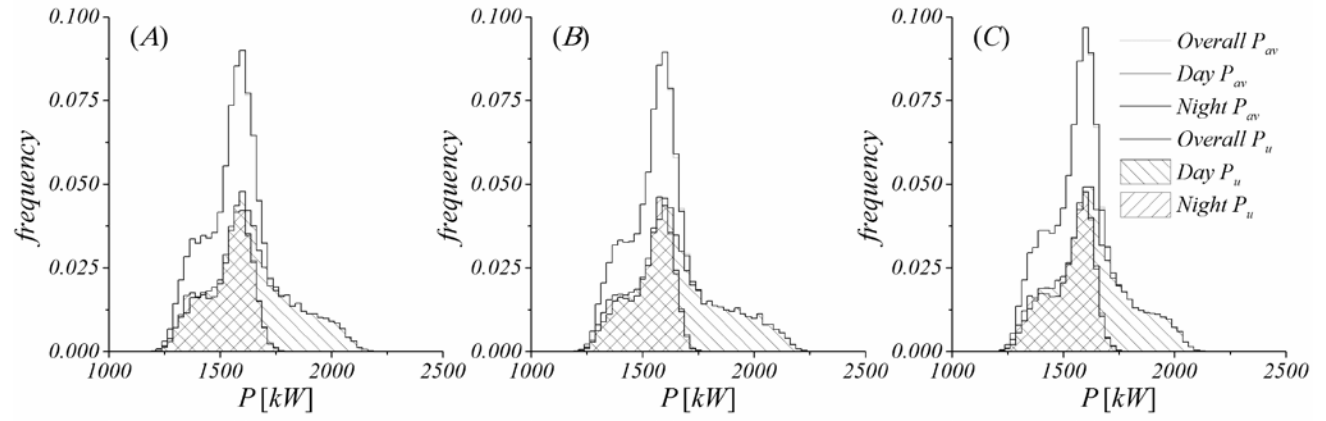

Figure 10. Total available P_{av} and used P_u power for configurations: Ξ_3^{DG} (*A*), Ξ_1^{DG} (*B*) and Ξ_2^{DG} (*C*)

With respect to the power generation, Figure 10 presents the histograms obtained for the overall available P_{av} and used P_u power from all the power sources (MS and DG) present in each of the three DG-integrated network configurations. The corresponding day and night histograms for P_{av} and P_u are also shown. The available power corresponds to the upper limit of the power that can eventually be used under specific operating conditions to satisfy a certain level of load. In the present case, it is possible to observe a central common peak (overall, day and night) in the aggregated P_{av} and P_u, that corresponds to the normally distributed MS power contribution. The lower frequencies in the range of power *1750-2250* [*kW*] are due to the absence of PV power supply during the night.

Furthermore, there are slight differences between P_{av} and P_u, explained by the fact that for the *25000* simulated operating scenarios the power available in the sources is not enough to satisfy the nodal loads. Indeed, the operating scenarios for which the total demand of power is completely satisfied (*ENS = 0*) are quite rare, with probabilities *0.0034*, *0.0034* and *0.0026* for each configuration Ξ_1^{DG}, Ξ_2^{DG} and Ξ_3^{DG}, respectively. These scenarios take place mainly during the low load range interval (night), in correspondence of which the OPF model 'decides' to use less than the available MS power privileging the use of DG power. This can be observed in Figure 11.

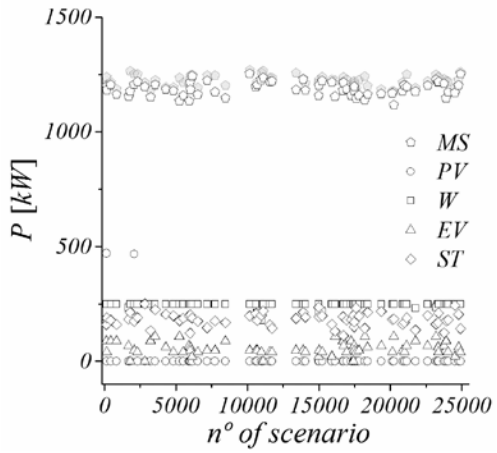

Figure 11. Scenarios of satisfied total load for configuration Ξ_3^{DG}

Figure 12 and Figure 13 report the empirical probability density functions (*pdfs*) of *ENS* and C_g and their respective day-night breakdown. The corresponding expected values, denoted by *EENS* and EC_g, and the standard deviation values are summarized in Table 12.

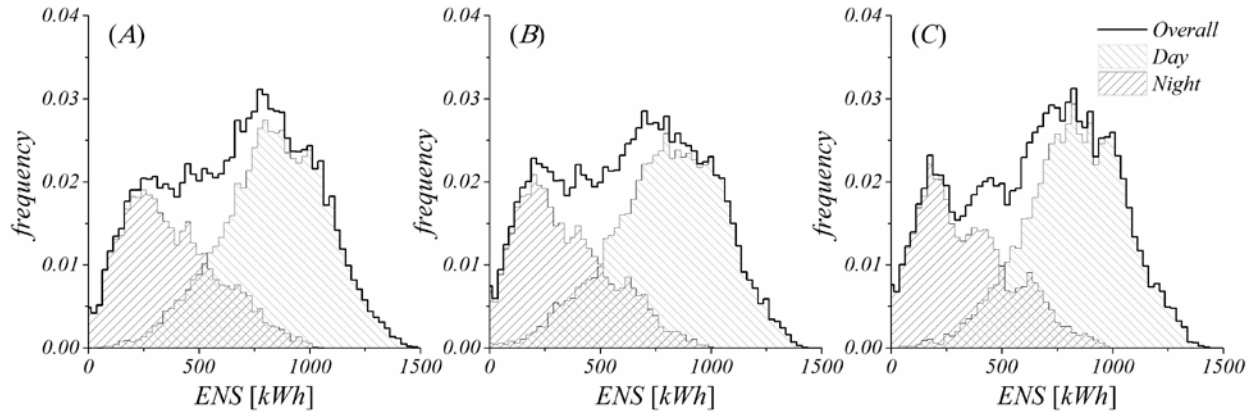

Figure 12. Empirical *ENS pdf* of configurations Ξ_3^{DG} (*A*), Ξ_1^{DG} (*B*) and Ξ_2^{DG} (*C*)

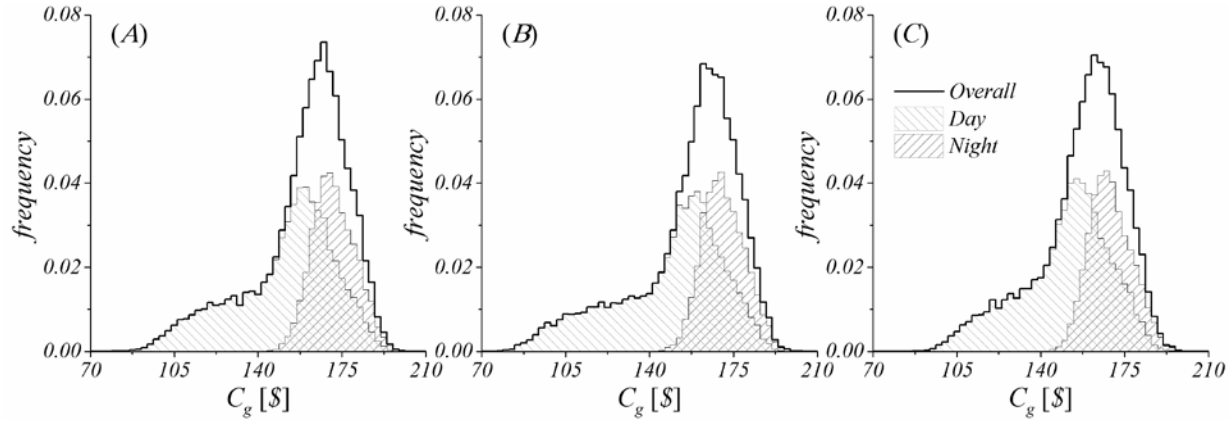

Figure 13. Empirical C_g *pdf* of configurations Ξ_3^{DG} (*A*), Ξ_1^{DG} (*B*) and Ξ_2^{DG} (*C*)

The outcome *pdf*s for *ENS* are coherent with the behavior of the total load and total available power. Low levels of power demand during the night range lead to having low levels of energy not supplied, even if no PV power is available. On the other hand, the increment of power demand during the day is considerably higher than the contribution of PV power, resulting in a frequency peak of high *ENS* values.

In the case of C_g, the overall performance is characterized by a reduction during the day interval. This can be explained by the incentive over DG power generation that promotes the use of renewable DG units above MS. Losing the PV

generation during the night, the corresponding incentive and revenues per *kWh* sold are lost, thus incrementing the global costs of the network.

Table 12. Expected values and standard deviations of *ENS* and C_g of DG-integrated networks

	[*kWh*]						[*$*]					
	Overall		*Day*		*Night*		*Overall*		*Day*		*Night*	
	EENS	$\sigma(ENS)$	*EENS*	$\sigma(ENS)$	*EENS*	$\sigma(ENS)$	EC_g	$\sigma(C_g)$	EC_g	$\sigma(C_g)$	EC_g	$\sigma(C_g)$
Ξ_1^{DG}	*656.45*	*323.72*	*841.41*	*224.68*	*350.91*	*211.31*	*158.25*	*18.63*	*150.86*	*19.11*	*170.45*	*8.84*
Ξ_2^{DG}	*676.38*	*319.98*	*851.92*	*235.19*	*388.21*	*214.55*	*157.47*	*22.34*	*148.62*	*23.28*	*172.28*	*8.76*
Ξ_3^{DG}	*642.14*	*323.99*	*814.48*	*249.13*	*353.91*	*209.68*	*159.86*	*20.29*	*151.93*	*21.15*	*172.89*	*8.93*

Figure 14 shows the variations of EC_g and *EENS* with respect to the uncertain variables that characterize the power output of each DG technology: *s*, *ws* and Q^{st}. The non-dominated solutions (Figure 8) are correspondingly presented. The arrows indicate the growth direction of each characteristic variable. It can be observed that the dispersions of the performance points (*EENS*, EC_g) for each characteristic variable represent independently the power output functions of the different DG technologies. Indeed, it is clear the linear tendency in the PV and ST technologies, given their linear power output functions. Similarly for W technology, the performance of both *EENS* and EC_g present the succession of increase, stationarity and decrease coherently to the behavior of the power output as function of the cut-in ws_{ci}, average ws_a and ws_{co} wind speeds (Figure 15(*A*)). In addition, the range of variation of (*EENS*, EC_g) corresponding to each uncertain variable depends on the installed capacity of each DG technology. For example, PV installed power is correspondingly higher in configurations { Ξ_1^{DG} , *149.53* [*kW*]}, { Ξ_3^{DG} ,*134.01* [*kW*]} and { Ξ_2^{DG} ,*117.32* [*kW*]}, and so it is its range of variation for (*EENS*,EC_g) as a function of *s*. Analogous is the case of ST, but the installed power and range of variation (for the batteries block considered) are higher for the sequence of configurations { Ξ_1^{DG} , *41* [*kW*]}, { Ξ_2^{DG} ,*19* [*kW*]} and { Ξ_3^{DG} , *1* [*kW*]}.

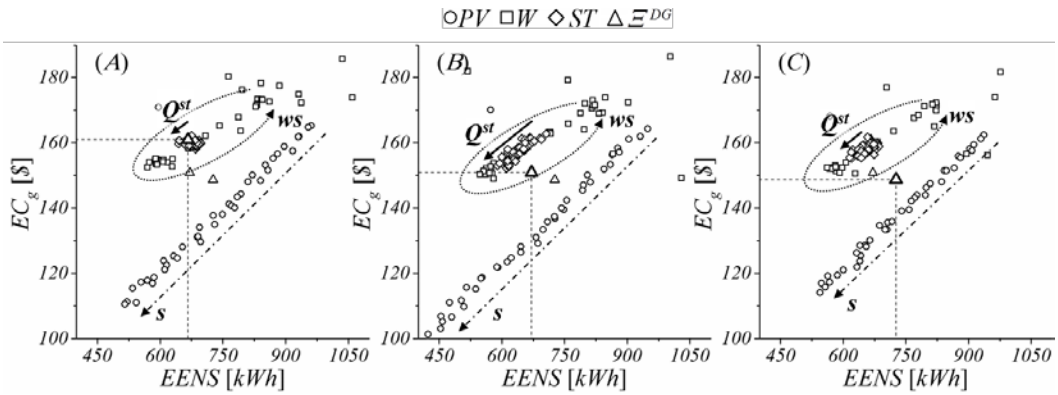

Figure 14. EC_g v/s *EENS* variations by DG-technology for configurations Ξ_3^{DG} (*A*), Ξ_1^{DG} (*B*) and Ξ_2^{DG} (*C*)

Considering the above, one might be led to conclude that *s* impacts more than the other variables the improvement of expected performance of the network, i.e. determines lower *EENS* and EC_g. However, its effects are being 'amplified' by the number of PV units installed in each DG-integrated network considered, not allowing a conclusive comparison with respect to *ws* and Q^{st}. Furthermore, the probabilities to obtain better performances (*EENS*,EC_g) by W and ST technologies are higher than by PV, as shown in Figure 15(*B*). The probability of occurrence of the extreme scenario in which the DG technologies generate at full capacity P_{max}, is remarkably higher in the case of W (≈*0.55*) than ST and PV (≈*0.025* and ≈*0.015*, respectively).

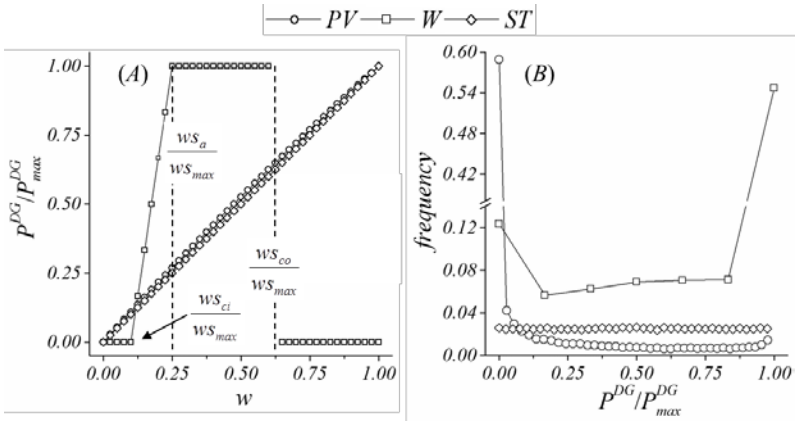

Figure 15. Normalized power output functions (*A*) and empirical probability distribution functions (*B*) per DG generation unit, $w \in \{s/s_{max}, ws/ws_{max}, Q^{st}/Q^{st}_{max}\}$

In order to compare the influence of the uncertain variables *s*, *ws* and Q^{st} on the network performance (*EENS*, EC_g), we focus on the reduction that results when, for each DG technology, the aggregated power output of the generation units is normalized by the maximum power capacity installed, i.e., $P^{pv}_{max} = P^{w}_{max} = P^{st}_{max} = 1\,[kW_{max}]$. This is done dividing the total differences $\Delta EENS(w)$ and $\Delta EC_g(w)$ ($w \in \{s/s_{max}, ws/ws_{max}, Q^{st}/Q^{st}_{max}\}$) by the maximum power installed per DG in the corresponding configuration.

Figure 16 shows the empirical reduction curves of *EENS* as functions of the uncertain variables of interest; the points of maximum unitary power output $1 \times kW_{max}$ are highlighted in Figure 16(*B*).

As before, the patterns of each DG power output function reflect into the behavior of $\Delta EENS$ for each uncertain variable. Moreover, in the cases of PV and W technologies the corresponding relations between $\Delta EENS$, *s* and *ws* are practically one-to-one, i.e., when these technologies operate individually at $1 \times kW_{max}$, *EENS* decreases approximately of *1* [*kW*]. It is important to notice that $\Delta EENS$ cannot be greater than *1* [*kW*], i.e., considering the singular effects of one of the variables *w*, *EENS* cannot diminish more than the maximum unitary power output. In the present case, for W and ST *EENS* is reduced more than *1* [*kW*] when *ws* or Q^{st} are in the ranges of generation of $1 \times kW_{max}$. This could be explained by their respective empirical *pdfs*, which are such to allow the realization of a broader spectrum of values *ws* and Q^{st} (Figure 15(*B*)).

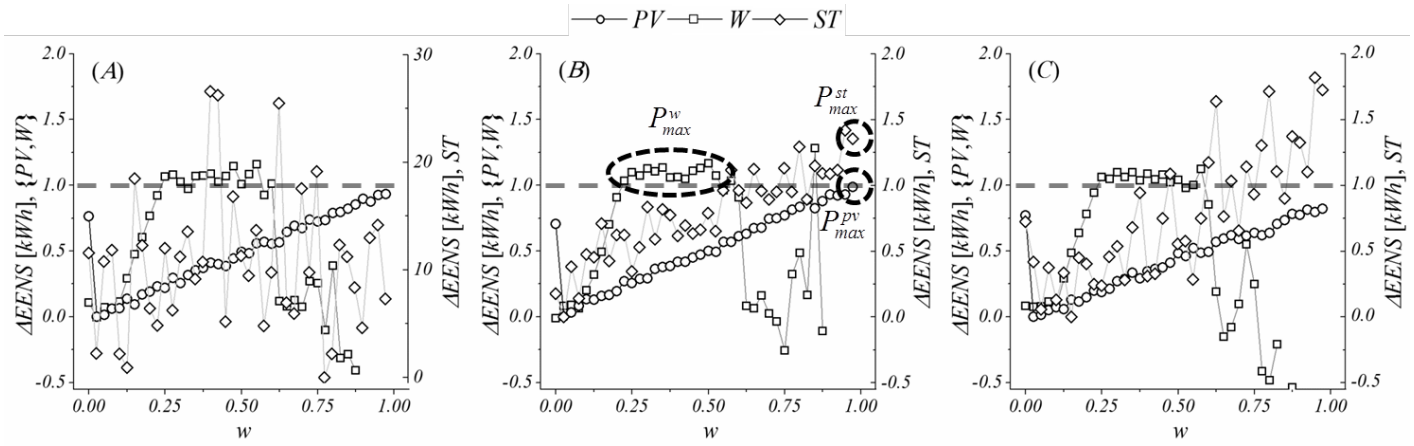

Figure 16. *EENS* reduction per $1 \times kW_{max}$ by DG-technology for configurations Ξ_3^{DG} (*A*), Ξ_1^{DG} (*B*) and Ξ_2^{DG} (*C*), $w \in \{s/s_{max}, ws/ws_{max}, Q^{st}/Q^{st}_{max}\}$

Recalling that in the case of ST, the uncertain variable of interest Q^{st} represents the level of charge of only one block of batteries of the corresponding DG-integrated network, it can be noticed that the variability of $\Delta EENS$ for this variable is considerably higher when the ST power installed is smaller. Indeed, the variability of the values of $\Delta EENS$ is directly related with the average power installed by block in the respective configurations, $\{\Xi_1^{DG}, 41\ [kW]\}$, $\{\Xi_2^{DG}, 19\ [kW]\}$ and $\{\Xi_3^{DG}, 1\ [kW]\}$, i.e., the variable Q^{st} has accordingly less influence on the network performance.

Analogously to the *EENS* analysis, Figure 17 report the empirical reduction curves of EC_g as function of the uncertain variables *s*, *ws* and Q^{st}. In this case, it can be noticed that the reduction ΔEC_g at maximum unitary power is slightly higher for PV than W and ST technologies, and more evident in configuration Ξ_1^{DG} which presents the larger amount of PV power installed *149.53* [*kW*] (Ξ_3^{DG} and Ξ_2^{DG}, *134.01* [*kW*] and *117.32* [*kW*], respectively).

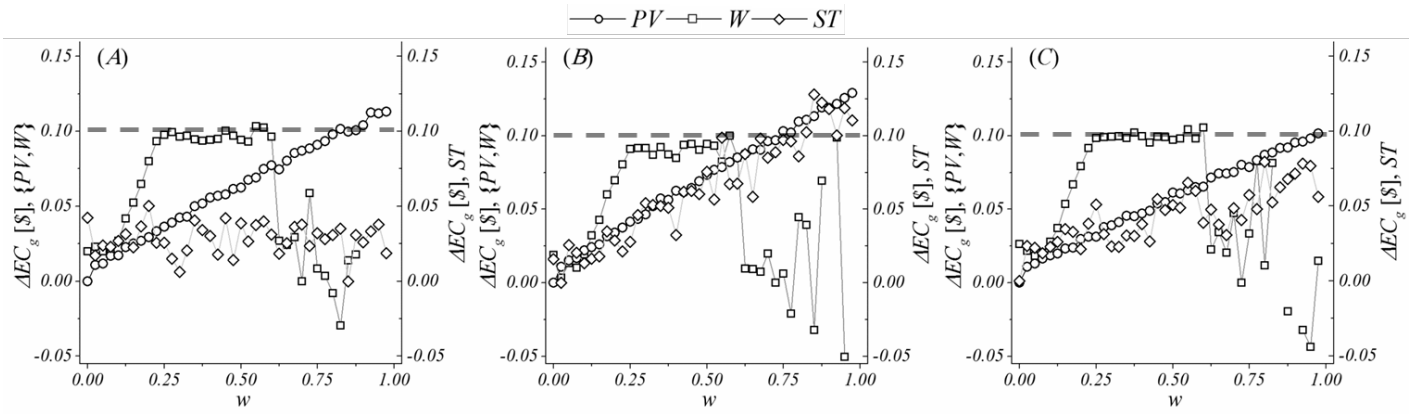

Figure 17. EC_g reduction per $1 \times kW_{max}$ by DG-technology for configurations Ξ_3^{DG} (*A*), Ξ_1^{DG} (*B*) and Ξ_2^{DG} (*C*), $w \in \{s/s_{max}, ws/ws_{max}, Q^{st}/Q^{st}_{max}\}$

As before, the variability of ΔEC_g for ST technology is accentuated when the power installed is lower, so that the impact of the variable Q^{st} over the network performance is not significant, as shown in Figure 17(*A*) for the DG-integrated network Ξ_3^{DG}.

The expected and standard deviation values of reductions *ΔEENS* and ΔEC_g obtained by the different DG technologies in the three network configurations considered are given in Table 13. On average, W technology leads to the highest reductions of *EENS* and EC_g, with comparable uncertainty (standard deviation) with respect to the other two technologies PV and ST. In addition, the probability that W operates at maximum power generation conditions implies that the occurrence of cases with more beneficial performance, i.e., around $E(\Delta EENS)+\sigma(\Delta EENS)$ and $E(\Delta EC_g)+\sigma(\Delta EC_g)$ is more frequent than the opposite cases (Figure 15). ST technology presents comparable expected values for the reductions *ΔEENS* and ΔEC_g with respect to W, but these values are highly variable with Q^{st}, conditioned by the amount of installed power in the block of batteries in the respective network configuration.

Table 13. Expected and standard deviation values of *ΔEENS* and ΔEC_g by DG-technology

		Ξ_1^{DG}			Ξ_2^{DG}			Ξ_3^{DG}		
		PV	*W*	*ST*	*PV*	*W*	*ST*	*PV*	*W*	*ST*[*]
ΔEENS [*kWh*]	$E(\cdot)$	*0.575*	***0.736***	*0.782*	*0.585*	***0.800***	*0.769*	*0.599*	***0.866***	*10.668*
	$\sigma(\cdot)$	*0.284*	***0.463***	*0.327*	*0.251*	***0.446***	*0.482*	*0.279*	***0.440***	*6.391*
	$\sigma(\cdot)/E(\cdot)$	*0.493*	*0.629*	*0.418*	*0.430*	*0.558*	*0.627*	*0.466*	*0.508*	*0.599*
ΔEC_g [$]	$E(\cdot)$	*0.023*	***0.067***	*0.064*	*0.019*	***0.075***	*0.043*	*0.021*	***0.073***	*0.028*
	$\sigma(\cdot)$	*0.036*	***0.037***	*0.035*	*0.028*	***0.034***	*0.018*	*0.032*	***0.035***	*0.010*
	$\sigma(\cdot)/E(\cdot)$	*1.541*	*0.547*	*0.547*	*1.491*	*0.450*	*0.430*	*1.550*	*0.474*	*0.374*

[*] ST technology is considered as 'not significant' for configuration Ξ_3^{DG}

The information reported in Table 13 is coherent and can be explained by looking back to the DG- integrated network configurations, especially Ξ_3^{DG} and Ξ_2^{DG} which minimize *EENS* and EC_g respectively. For all of the three configurations Ξ_1^{DG}, Ξ_2^{DG} and Ξ_3^{DG}, the number of W generation units installed is the same (5 units) and, thus, the differences in their performances are mainly due to differences in PV and ST. Indeed, on one hand in configuration Ξ_2^{DG} (min EC_g) the total average ST power installed is higher than in Ξ_3^{DG} (*160.00* and *144.00* [*kW*], respectively) and privileged over PV (*117.32* and *134.01* [*kW*], respectively), implying higher expected reductions ΔEC_g and, therefore, lower values of EC_g performances. On the other hand, in configuration Ξ_3^{DG} (min *EENS*) the total average PV power installed is higher than in Ξ_2^{DG}, but not privileged over ST. This can be due to the smaller differences between the

expected values of $\Delta EENS$ of ST and PV technologies, with respect to ΔEC_g that instead of favoring one technology tends to balance them.

4. CONCLUSIONS

We have presented a sensitivity analysis of a combined Monte Carlo and optimal power flow simulation model for the performance evaluation of a renewable distributed generation network. The inherent uncertain behavior of renewable energy sources, the fluctuations in the loads and the possibility of failures of network components are taken into account for emulating the stochastic operating scenarios. The sensitivity analysis is performed individually over the characteristic uncertain variables of the DG technologies of interest, PV, W and ST. The respective impacts of the solar irradiance, the wind speed and the storage level of one block of storage devices are evaluated over the two DG-integrated network performance functions considered, global cost and energy not supplied.

Three different DG-integrated network configurations have been considered for the exemplification of the analysis, selected among those of the Pareto set obtained by the authors in a previous work of multi-objective optimization of resource allocation by a non-dominated sorting genetic algorithm. The results obtained show the coherence of the outcome *pdf*s for *ENS* and C_g with respect to the day-night behavior of the total load and available power, and how the incentive and revenues per renewable *kWh* promote the use of renewable DG units. The introduction of the empirical reduction curves of *EENS* and EC_g, as functions of the uncertain variables of interest, allows to compare their impact independent of the 'amplifying' effect produced by the number of DG units installed. Moreover, the integrated analysis of the empirical reduction curves $\Delta EENS$ and ΔEC_g for each uncertain variable and their respective empirical *pdf* enables trade-offs between possible benefits and probability of occurrence.

References

[1] **A. Alarcon-Rodriguez, G. Ault, and S. Galloway, "Multi-objective planning of distributed energy resources: A review of the state-of-the-art," *Renewable and Sustainable Energy Reviews,* vol. 14, pp. 1353 - 1366, 2010.**

[2] **G. N. Koutroumpezis and A. S. Safigianni, "Optimum allocation of the maximum possible distributed generation penetration in a distribution network," *Electric Power Systems Research,* vol. 80, pp. 1421 - 1427, 2010.**

[3] **V. F. Martins and C. L. T. Borges, "Active Distribution Network Integrated Planning Incorporating Distributed Generation and Load Response Uncertainties," *Power Systems, IEEE Transactions on,* vol. 26, pp. 2164 -2172, nov. 2011.**

[4] **M. Raoofat, "Simultaneous allocation of DGs and remote controllable switches in distribution networks considering multilevel load model," *International Journal of Electrical Power and Energy Systems,* vol. 33, pp. 1429 - 1436, 2011.**

[5] **H. Falaghi, C. Singh, M.-R. Haghifam, and M. Ramezani, "DG integrated multistage distribution system expansion planning," *International Journal of Electrical Power and Energy Systems,* vol. 33, pp. 1489 - 1497, 2011.**

[6] **S.-H. Lee and J.-W. Park, "Selection of Optimal Location and Size of Multiple Distributed Generations by Using Kalman Filter Algorithm," *Power Systems, IEEE Transactions on,* vol. 24, pp. 1393 -1400, aug. 2009.**

[7] **Y. M. Atwa, E. F. El-Saadany, M. M. A. Salama, and R. Seethapathy, "Optimal Renewable Resources Mix for Distribution System Energy Loss Minimization," *Power Systems, IEEE Transactions on,* vol. 25, pp. 360 -370, feb. 2010.**

[8] **W. El-Khattam, K. Bhattacharya, Y. Hegazy, and M. M. A. Salama, "Optimal investment planning for distributed generation in a competitive electricity market," *Power Systems, IEEE Transactions on,* vol. 19, pp. 1674 - 1684, aug. 2004.**

[9] **W. El-Khattam, Y. G. Hegazy, and M. M. A. Salama, "An integrated distributed generation optimization model for distribution system planning," *Power Systems, IEEE Transactions on,* vol. 20, pp. 1158 - 1165, may 2005.**

[10] **Z. Liu, F. Wen, and G. Ledwich, "Optimal Siting and Sizing of Distributed Generators in Distribution Systems Considering Uncertainties," *Power Delivery, IEEE Transactions on*, vol. 26, pp. 2541 -2551, oct. 2011.**

[11] **R. Mena, M. Hennebel, Y. Li, C. Ruiz, and E. Zio, "A Risk-Based Simulation and Multi-Objective Optimization Framework for the Integration of Distributed Renewable Generation and Storage," *Renewable and Sustainable Energy Reviews*, (Under Review) 2013.**

[12] **H. Ren and W. Gao, "A MILP model for integrated plan and evaluation of distributed energy systems," *Applied Energy*, vol. 87, pp. 1001 - 1014, 2010.**

[13] **H. Ren, W. Zhou, K. a. t. Nakagami, W. Gao, and Q. Wu, "Multi-objective optimization for the operation of distributed energy systems considering economic and environmental aspects," *Applied Energy*, vol. 87, pp. 3642 - 3651, 2010.**

[14] **A. Alarcon-Rodriguez, E. Haesen, G. Ault, J. Driesen, and R. Belmans, "Multi-objective planning framework for stochastic and controllable distributed energy resources," *Renewable Power Generation, IET*, vol. 3, pp. 227 -238, june 2009.**

[15] **Y. Hegazy, "Adequacy assessment of distributed generation systems using Monte Carlo simulation," *Power Systems, IEEE Transactions on*, vol. 18, pp. 48-52, 2003.**

[16] **Y. Li and E. Zio, "Uncertainty analysis of the adequacy assessment model of a distributed generation system," *Renewable Energy*, vol. 41, pp. 235 - 244, 2012.**

[17] **Y.-F. Li and E. Zio, "A multi-state model for the reliability assessment of a distributed generation system via universal generating function," *Reliability Engineering & System Safety*, vol. 106, pp. 28-36, 2012.**

[18] **J. Zhao and J. Foster, "Flexible transmission network planning considering distributed generation impacts," *Power Systems, IEEE Transactions on*, vol. 26, pp. 1434-1443, 2011.**

[19] **K. Purchala and L. Meeus, "Usefulness of DC power flow for active power flow analysis," *Power Engineering …*, 2005.**

[20] **R. Billinton, R. Allan, and R. Allan, "Reliability evaluation of power systems," 1996.**

[21] **IEEE Power and Energy Society. *Distribution Test Feeders*. Available: http://ewh.ieee.org/soc/pes/dsacom/testfeeders/index.html**

[22] **W. H. Kersting, "Radial distribution test feeders," *IEEE Transactions on Power Systems*, vol. 6, pp. 975-985, 1991.**

[23] **R. Webster, "Can the electricity distribution network cope with an influx of electric vehicles?," *Journal of Power Sources*, pp. 217-225, 1999.**

[24] **F. Pilo, G. Celli, S. Mocci, and G. G. Soma, "Active distribution network evolution in different regulatory environments," in *Power Generation, Transmission, Distribution and Energy Conversion (MedPower 2010), 7th Mediterranean Conference and Exhibition on*, ed, 2010, pp. 1 -8.**

[25] **K. Zou, A. P. Agalgaonkar, K. M. Muttaqi, and S. Perera, "Multi-objective optimisation for distribution system planning with renewable energy resources," in *Energy Conference and Exhibition (EnergyCon), 2010 IEEE International*, ed, 2010, pp. 670 -675.**